Journal of Solid State Chemistry 181 (2008) 2705–2712

Contents lists available at ScienceDirect

Journal of Solid State Chemistry

journal homepage: www.elsevier.com/locate/jssc

Synthesis and characterization of the K_2NiF_4 phases $La_{1+x}Sr_{1-x}Co_{0.5}Fe_{0.5}O_{4-\delta}$ ($x = 0$, 0.2)

H. El Shinawi, C. Greaves *

School of Chemistry, University of Birmingham, Birmingham B15 2TT, UK

ARTICLE INFO

Article history:
Received 28 April 2008
Received in revised form
17 June 2008
Accepted 19 June 2008
Available online 22 June 2008

Keywords:
K_2NiF_4 structure
$La_{1+x}Sr_{1-x}C_{0.5}Fe_{0.5}O_{4-\delta}$
Oxide ion vacancy
Neutron powder diffraction
Antiferromagnetic ordering

ABSTRACT

The K_2NiF_4 phases $LaSrCo_{0.5}Fe_{0.5}O_4$ and $La_{1.2}Sr_{0.8}Co_{0.5}Fe_{0.5}O_4$, and their reduced forms $LaSrCo_{0.5}Fe_{0.5}O_{3.75}$ and $La_{1.2}Sr_{0.8}Co_{0.5}Fe_{0.5}O_{3.85}$, have been successfully prepared by solid-state reactions, followed by reduction in 10% H_2/N_2 in order to produce oxygen-deficient materials. All materials crystallize in a tetragonal K_2NiF_4 structure (space group $I4/mmm$) with Co and Fe randomly distributed over the B-sites of the structure. Mössbauer spectra have confirmed the trivalent state of Fe in these materials. In the reduced materials, oxide ion vacancies are confined to the equatorial planes of the K_2NiF_4 structure and the Co is present almost entirely as Co^{2+} ions; low-temperature neutron powder diffraction data reveal that these reduced phases are antiferromagnetically ordered with a tetragonal noncollinear arrangement of the moments. The Co^{3+} ions, present in stoichiometric $LaSrCo_{0.5}Fe_{0.5}O_4$ and $La_{1.2}Sr_{0.8}Co_{0.5}Fe_{0.5}O_4$, inhibit magnetic order and are assumed to be in the low-spin state.

1. Introduction

Perovskite-type oxides which are able to support both mobile oxygen ions and electronic conductivity over a wide range of oxygen partial pressures are of great interest as electrode materials in solid oxide fuel cells (SOFCs), oxygen separation membranes and catalysts. For this reason, the mixed conducting perovskites $La_{1-x}Sr_xCo_{1-y}Fe_yO_{3-\delta}$ have been widely studied [1–3]. Recently, some interest has been focused on related Ruddlesden Popper phases $(La/Sr)_{n+1}(Co/Fe)_nO_{3n+1}$ which exhibit variable oxygen nonstoichiometry along with structural stability at high temperatures in reducing conditions; this has been linked to the flexibility of the cations to accommodate a range of transition metal coordination environments. Of these systems, the parent material $Sr_3Fe_2O_{7-\delta}$ has a tetragonal structure (space group $I4/mmm$) and exhibits oxygen deficiency $\delta \leqslant 1$. The sample with $\delta = 1$ was prepared in 5% H_2/N_2 atmosphere at 700 °C and showed no variation in the crystal structure symmetry [4]. Manthiram et al. [5] have studied structural stability and oxygen permeation properties of $Sr_{3-x}La_xFe_{2-y}Co_yO_{7-\delta}$, which retains tetragonal symmetry with temperatures up to 1000 °C in the oxygen partial pressure range 10^{-5}–0.21 atm. Other related systems which showed high ability to sustain low oxygen content without change in crystal structure symmetry are $Sr_3FeCoO_{7-\delta}$ ($\delta \leqslant 1.55$) [6], $Sr_3LaFe_{1.5}Co_{1.5}O_{8.25}$ and $Sr_3LaFe_{1.5}Co_{1.5}O_{7.5}$ [7].

The stoichiometric materials $LaSrCo_{1-x}Fe_xO_4$ have been synthesized by Tabuchi et al. [8]. The study involved detailed structural and magnetic characterization, although the half-doped member $LaSrCo_{0.5}Fe_{0.5}O_4$ has not been characterized. We report here the synthesis and characterization of the $n = 1$ Ruddlesden Popper phases $LaSrCo_{0.5}Fe_{0.5}O_4$ and $La_{1.2}Sr_{0.8}Co_{0.5}Fe_{0.5}O_4$ and their reduced forms $LaSrCo_{0.5}Fe_{0.5}O_{3.75}$ and $La_{1.2}Sr_{0.8}Co_{0.5}Fe_{0.5}O_{3.85}$; the reduction has been achieved in 10% H_2/N_2 at 800 °C with no variation in the crystal structure symmetry; moreover, TG data indicate structural stability of these materials in this atmosphere up to 1000 °C. The present study involves structural and magnetic characterization of these materials.

2. Experimental

$LaSrCo_{0.5}Fe_{0.5}O_{4-\delta}$ (LA1) and $La_{1.2}Sr_{0.8}Co_{0.5}Fe_{0.5}O_{4-\delta}$ (LA12) were prepared using conventional solid-state reactions involving analytical grade $SrCO_3$, La_2O_3, Co_3O_4 and Fe_2O_3 (all previously heated in air at 800 °C for 12 h to remove residual water hydroxide or carbonate). Attempts to effect the reaction in air were unsuccessful, since some perovskite impurities were produced, and a two-step synthesis procedure was therefore adopted. Stoichiometric amounts of starting materials were initially intimately mixed, pressed into pellets and calcined at 1350 °C for 30 h under a N_2 atmosphere. After grinding, the samples were

* Corresponding author. Fax: +44 121 414 4442.
E-mail address: c.greaves@bham.ac.uk (C. Greaves).

0022-4596/$ - see front matter © 2008 Elsevier Inc. All rights reserved.
doi:10.1016/j.jssc.2008.06.039

subsequently heated in air (at 800 °C for 12 h) or flowing 10% H_2/N_2 gas (at 800 °C for 12 h) in order to prepare the "oxidized" samples (LA1-ox and LA12-ox) and the "reduced" samples (LA1-red and LA12-red), respectively.

X-ray powder diffraction (XRD) data were collected using a Siemens D5000 diffractometer in transmission mode, employing Cu$K\alpha_1$ radiation from a germanium monochromator. Neutron powder diffraction (NPD) data were collected at room temperature and 5 K on the D2B diffractometer at the Institute Laue Langevin, Grenoble, using a wavelength of 1.594 Å. Rietveld refinement was performed on the powder diffraction data using the GSAS suite of programs [9] employing a pseudo-Voigt peak shape for the oxidized materials and a combination of pseudo-Voigt and Finger–Cox–Jephcoat functions for the reduced samples. This function was necessary to obtain a good fit to the experimental data and indicates significant anisotropic peak broadening in these materials. A small correction for preferred orientation was also allowed in the refinement. Magnetic data were collected using a Quantum Design PPMS magnetometer in the temperature range 5–300 K. Zero-field-cooled (ZFC) and field-cooled (FC) data were collected on warming using an applied field of 0.3 T. ^{57}Fe Mössbauer spectra were recorded at 298 K with a microprocessor-controlled Mössbauer spectrometer using a 25 mCi ^{57}Co/Rh source. The spectra were computer fitted and isomer shifts are reported relative to metallic iron at room temperature.

3. Results

3.1. Structural characterization

XRD patterns indicated that all samples were single-phase with no evidence of product impurities or starting materials. The patterns were readily indexed on a body-centred tetragonal unit cell, consistent with a structure related to that of K_2NiF_4. Although structural refinements based on XRD data confirmed the structure ($I4/mmm$ space group), the refinements were insensitive to oxygen stoichiometry and the oxide ion sites could be fixed at full occupancy.

NPD data collected at room temperature were used to probe more reliably the oxygen content and defect structure of these phases. Rietveld profile refinement of the high-intensity powder diffraction (HIPD) data was performed and the profile-fit and difference patterns of the Rietveld analysis of different samples are shown in Fig. 1; structural data and some selected bond lengths are given in Tables 1 and 2, respectively.

The O2 apical (axial) oxygen sites (0,0,z) were allowed to vibrate anisotropically and all samples had higher displacements perpendicular to the (Co/Fe)–O bond (Table 1). This is quite normal for this layered structure, but might also be augmented by the different bond requirements of Co and Fe in this mixed oxide. Split oxide ion sites have previously been invoked in the analysis of $LaSrCoO_{3.5-x}$ [10]. Oxide ion vacancies created in

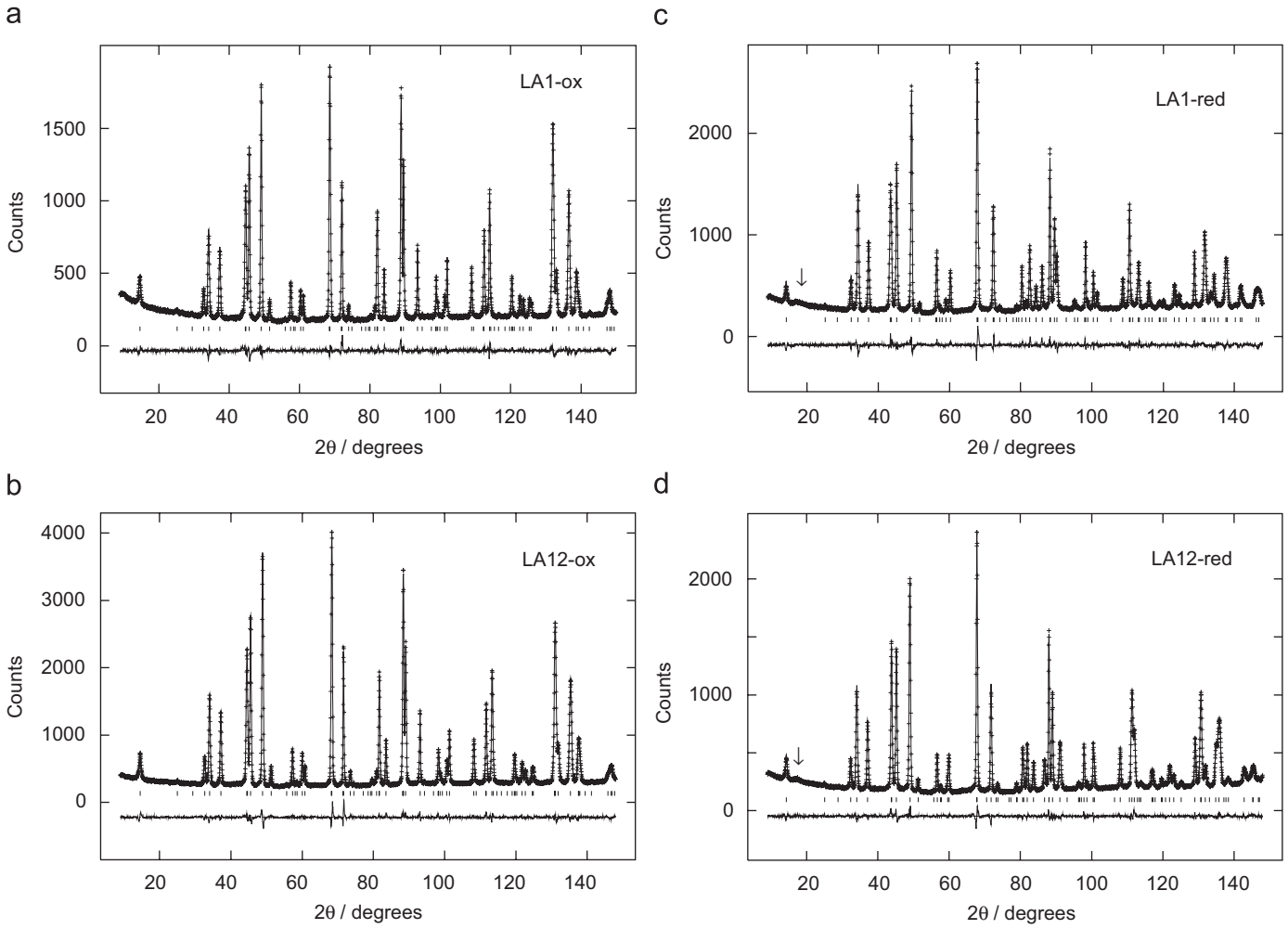

Fig. 1. Observed, calculated and difference profiles for NPD data collected at room temperature: (a) LA1-ox, (b) LA12-ox, (c) LA1-red and (d) LA12-red. The arrows in (c) and (d) show diffuse peaks that may indicate short-range magnetic ordering.

Table 1
Structural results from refinement using room temperature neutron diffraction data

Atom	x	y	z	$100 \times U_{iso}$ (Å^2)	Occupancy	x	y	z	$100 \times U_{iso}$ (Å^2)	Occupancy
LA1-ox: $LaSrCo_{0.5}Fe_{0.5}O_4$, space group $I4/mmm$						LA12-ox: $La_{1.2}Sr_{0.8}Co_{0.5}Fe_{0.5}O_4$, space group $I4/mmm$				
Co/Fe	0	0	0	0.110(3)	0.5/0.5	0	0	0	0.303(3)	0.5/0.5
La/Sr	0	0	0.3596(8)	0.165(2)	0.5/0.5	0	0	0.3600(3)	0.364(2)	0.6/0.4
O1	0.5	0	0	0.329(2)	1	0.5	0	0	0.616(2)	1
O2	0	0	0.1659(5)	1.09*	1	0	0	0.1677(9)	1.62*	1
*$U_{11} = 1.249(3)$ Å^2; $U_{22} = 1.249(3)$ Å^2; $U_{33} = 0.77(9)$ Å^2						*$U_{11} = 1.844(4)$ Å^2; $U_{22} = 1.844(4)$ Å^2; $U_{33} = 1.18(8)$ Å^2				
$a = 3.83900(6)$ Å; $c = 12.56764(2)$ Å wRp = 0.0314; Rp = 0.0237; $\chi^2 = 2.423$						$a = 3.85523(6)$ Å; $c = 12.60714(2)$ Å wRp = 0.0352; Rp = 0.0261; $\chi^2 = 3.226$				
LA1-red: $LaSrCo_{0.5}Fe_{0.5}O_{3.732(8)}$, space group $I4/mmm$						LA12-red: $La_{1.2}Sr_{0.8}Co_{0.5}Fe_{0.5}O_{3.880(8)}$, space group $I4/mmm$				
Co/Fe	0	0	0	0.75(4)	0.5/0.5	0	0	0	0.309(2)	0.5/0.5
La/Sr	0	0	0.3571(5)	0.873(2)	0.5/0.5	0	0	0.3593(0)	0.358(2)	0.6/0.4
O1	0.5	0.0509(6)	0	0.70(5)	0.433(2)	0.5	0.0333(7)	0	0.504(4)	0.470(2)
O2	0	0	0.1697(1)	1.81*	1	0	0	0.1710(2)	1.55*	1
*$U_{11} = 2.21(4)$ Å^2; $U_{22} = 2.21(4)$ Å^2; $U_{33} = 1.03(7)$ Å^2						*$U_{11} = 1.953(3)$ Å^2; $U_{22} = 1.953(3)$ Å^2; $U_{33} = 0.74(8)$ Å^2				
$a = 3.82375(4)$ Å; $c = 12.96352(2)$ Å wRp = 0.0345; Rp = 0.0256; $\chi^2 = 3.971$						$a = 3.84893(8)$ Å; $c = 12.84061(3)$ Å wRp = 0.0303; Rp = 0.0234; $\chi^2 = 2.294$				

Table 2
Selected bond lengths (Å) for the refined phases

Bond	$LaSrCo_{0.5}Fe_{0.5}O_4$	$La_{1.2}Sr_{0.8}Co_{0.5}Fe_{0.5}O_4$	$LaSrCo_{0.5}Fe_{0.5}O_{3.732(8)}$	$La_{1.2}Sr_{0.8}Co_{0.5}Fe_{0.5}O_{3.880(8)}$
Co/Fe–O1	1.919(5) [× 4]	1.927(6) [× 4]	1.921(8) [× 8][a]	1.928(7) [× 8][a]
Co/Fe–O2	2.085(5) [× 2]	2.115(3) [× 2]	2.200(1) [× 2]	2.195(9) [× 2]
La/Sr–O1	2.606(7) [× 4]	2.613(5) [× 4]	2.804(8) [× 4][a]	2.734(5) [× 4][a]
			2.525(6) [× 4][a]	2.547(9) [× 4][a]
La/Sr–O2	2.733(6) [× 4]	2.748(5) [× 4]	2.726(1) [× 4]	2.749(3) [× 4]
	2.434(8) [× 1]	2.423(5) [× 1]	2.429(8) [× 1]	2.417(6) [× 1]

[a] Splitting of O1 sites gives twice the number of bonds compared with the ideal site.

the reduced samples were disordered and confined to the (Co/Fe)O_2 planes of the K_2NiF_4 structure with an associated twisting of the (Co/Fe)O_6 octahedra around the z-axis; this transforms the oxide ion at (0.5,0,0) to the split position (0.5,y,0), where y appears to increase with the concentration of oxygen vacancies (Table 1). The retention of the tetragonal symmetry under reduction with an equatorial distribution of oxide ion vacancies has also been observed in $LaSrCoO_{3.5-x}$ phases [10]. Attempts to refine models with either ordered oxide vacancies in larger unit cells (in a manner similar to $Ca_2MnO_{3.5}$ [11] or $La_{1.6}Sr_{0.4}NiO_{3.47}$ [12]) or vacancy distribution between both axial and equatorial sites in a tetragonal unit cell (in a manner similar to $NdSrCuO_{3.56}$ [13]) were unsuccessful, and provided confirmation of the model with a disordered distribution of vacancies in only equatorial sites.

The overall refined stoichiometries for LA1-ox, LA12-ox, LA1-red and LA12-red are $LaSrCo_{0.5}Fe_{0.5}O_4$, $La_{1.2}Sr_{0.8}Co_{0.5}Fe_{0.5}O_4$, $LaSrCo_{0.5}Fe_{0.5}O_{3.732(8)}$ and $La_{1.2}Sr_{0.8}Co_{0.5}Fe_{0.5}O_{3.880(8)}$, respectively. No oxygen excess has been observed in the oxidized materials. These stoichiometries are consistent with thermogravimetric analysis (reduction of La1-ox and La12-ox in 10% H_2/N_2 at 800 °C; Fig. 2), which indicated compositions of $LaSrCo_{0.5}Fe_{0.5}O_{3.74(2)}$ and $La_{1.2}Sr_{0.8}Co_{0.5}Fe_{0.5}O_{3.85(2)}$ for the reduced phases if the oxidized materials are stoichiometric in oxygen. The refined stoichiometry and vacancy distribution in the reduced phases suggest the formation of (Co/Fe)O_x polyhedra of coordination lower than 6, similar to those observed in $LaSrCoO_{3.5-x}$ [10]. It can be also noted that the polyhedra exhibit a significant elongation along the c-axis in all phases, being more pronounced in the reduced samples (M–O2/M–O1 is 1.09, 1.1, 1.14 and 1.15 in LA1-ox, LA12-ox, LA12-red and LA1-red, respectively).

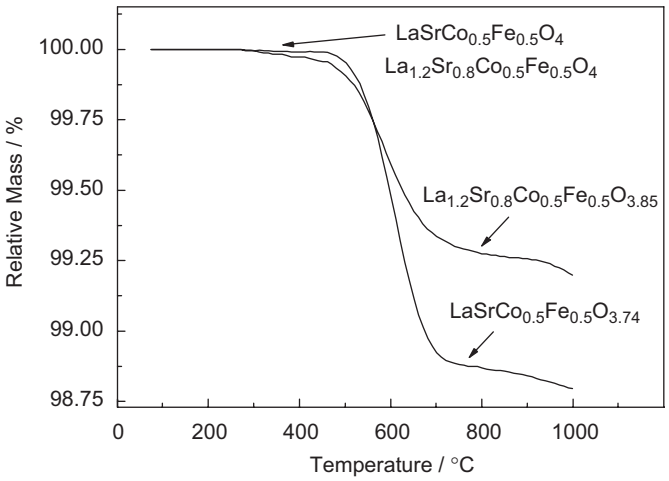

Fig. 2. Thermogravimetric data for the reduction of La1-ox and LA12-ox using 10% H_2 in N_2.

Fig. 3 shows ^{57}Fe Mössbauer spectra of LA12-ox and LA12-red at room temperature. The solid curve in the figure shows the result of least-squares computer fitting of lorentzian curves. A one-doublet computer fit yielded quadrupole splitting values of 1.09 and 1.49 mm s^{-1} for LA12-ox and LA12-red, respectively, and an isomer shift of 0.32 mm s^{-1} for both samples. The observed isomer shift and quadrupole splitting values are characteristic of Fe^{3+} in distorted octahedral oxygen coordination [14,15]. For LA12-ox, the relatively high quadrupole splitting may be related to a slight distortion (M–O2/M–O1 is 1.10) and/or covalency effects.

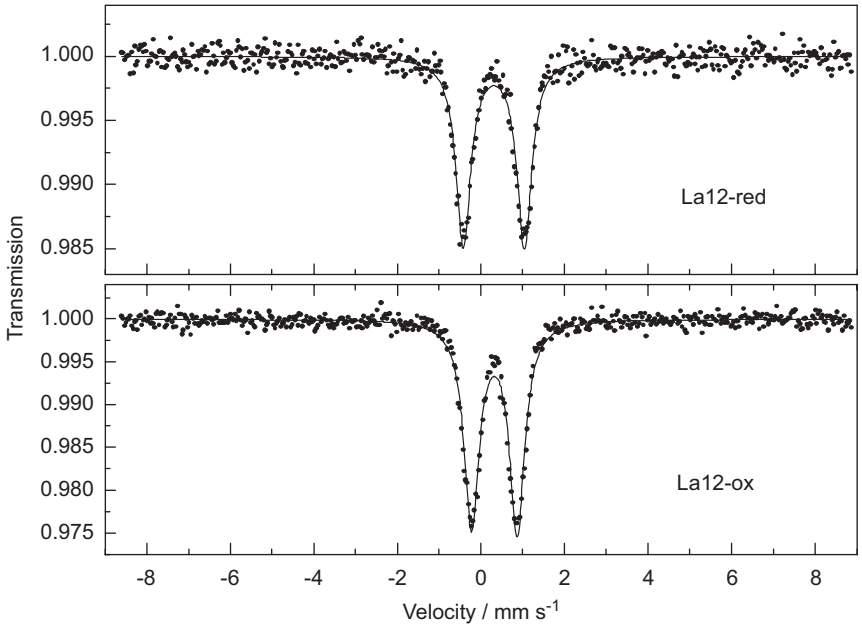

Fig. 3. ^{57}Fe Mossbauer spectra of LA12-ox and LA12-red at room temperature.

The higher quadrupole splitting of the reduced sample ($1.49\,mm\,s^{-1}$) reflects an enhanced distortion which is consistent with an increased elongation along *c* (*M*–O2/*M*–O1 is 1.14) and the presence of oxygen vacancies.

Given the presence of Fe^{3+} in all phases, Co ions in LA1-ox are totally in the trivalent state (Co^{3+}), whereas 40% of the Co ions in LA12-ox are in the divalent state (Co^{2+}). The oxygen contents in the reduced samples are consistent with phases containing pure Co^{2+} and Fe^{3+} ions (LA1-red and LA12-red Co oxidation states: 1.92(2) and 2.12(2) from refinement, 1.96(8) and 2.00(8) from TG). The nominal compositions (based on Co^{2+}) will now be adopted for LA1-red and LA12-red: $LaSrCo_{0.5}Fe_{0.5}O_{3.75}$ and $La_{1.2}Sr_{0.8}Co_{0.5}Fe_{0.5}O_{3.85}$, respectively. It is interesting to note that similar K_2NiF_4 phases containing Co mainly in the divalent state, such as La_2CoO_4 and $LaSrCoO_{3.5-x}$, undergo room temperature topotactic oxidation in air and are stable only under inert atmospheres [10,16]. In contrast, the Co^{2+}-containing phases studied here ($LaSrCo_{0.5}Fe_{0.5}O_{3.75}$ and $La_{1.2}Sr_{0.8}Co_{0.5}Fe_{0.5}O_{3.85}$) do not show such reactivity toward atmospheric oxygen at ambient temperatures.

3.2. Magnetic characterization

Fig. 4 shows the temperature dependence of the magnetic susceptibility of different samples. The oxidized materials generally show higher magnetization than the reduced ones, with a paramagnetic enhancement of susceptibility at low temperatures. A distinct divergence between ZFC and FC susceptibilities for the oxidized samples is suggestive of spin glass behaviour. As shown in the insets of Fig. 4, susceptibilities of the reduced samples (LA1-red and LA12-red) show broad antiferromagnetic (AFM)-like peaks around or just below room temperature indicating AFM ordering in these materials. Again, divergence between ZFC and FC data is seen, and may indicate a small ferromagnetic (FM) component due to canting of the moments. The diffuse peaks which can be seen around $2\theta = 17^{\circ}$ in the room temperature NPD patterns of the reduced samples (see arrows in Fig. 1(c) and (d)) are consistent with the existence of short-range magnetic order at this temperature, although no magnetic splitting is observed in the Mössbauer data of LA12-red.

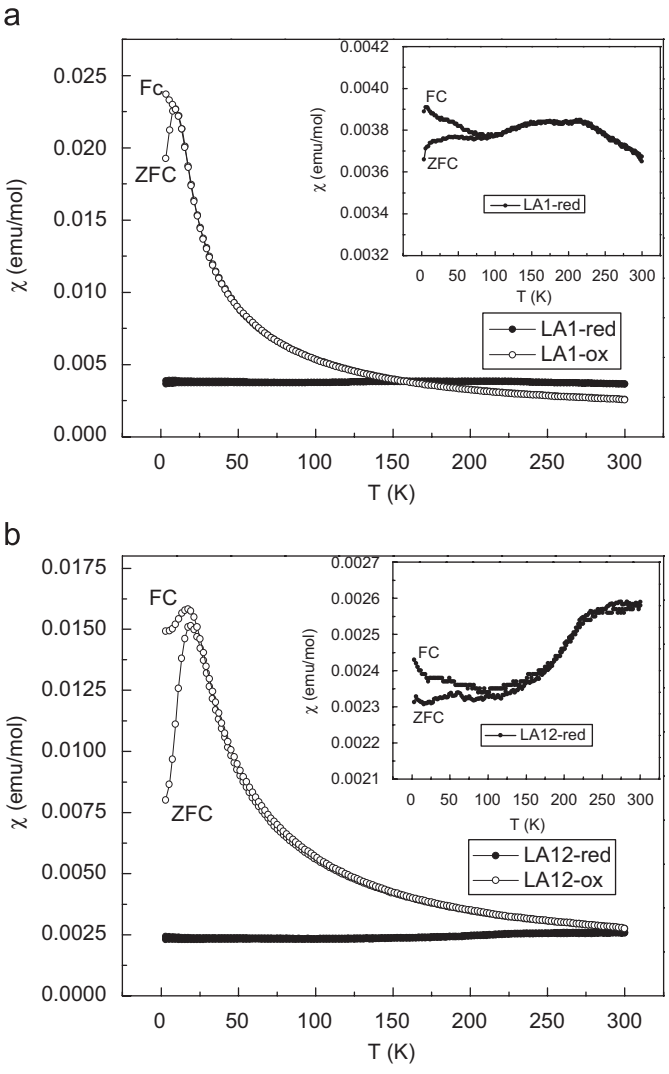

Fig. 4. Variation of magnetic susceptibility (ZFC and FC) with temperature.

NPD data collected at 5 K have confirmed that the reduced samples are magnetically ordered at this temperature. Compared with data sets collected at room temperature, a series of additional Bragg reflections were clearly observed for LA1-red and LA12-red data at 5 K (see Fig. 5). These additional Bragg reflections could be indexed with a primitive tetragonal cell with lattice parameters $a_{\text{magnetic}} = \sqrt{2} \times a_{\text{nuclear}}$ and $c_{\text{magnetic}} = c_{\text{nuclear}}$. Several models of AFM order were examined including alignments of moments parallel to the z-axis and those with moments confined to the xy plane. Two collinear in-plane models related to La_2CuO_4 and $La_2NiO_{4+\delta}$ magnetic structures, frequently occur in ordered K_2NiF_4-type antiferromagnets; both models consist of alternate FM sheets coupled antiferromagnetically, with the moments aligned either parallel (La_2CuO_4-type structure) or perpendicular ($La_2NiO_{4+\delta}$-type structure) to the FM planes [17,18]. Fig. 5 shows a very strong magnetic peak at $2\theta \sim 17^\circ$, which corresponds to the (100) reflection of the magnetic supercell. This observation requires a major FM component of the moments to be perpendicular to $\langle 100 \rangle$ directions, and is therefore consistent with a collinear La_2CuO_4-type magnetic order previously reported, for example, for $LaAFeO_4$ (A = Ca, Sr) [19,20]. However, there was no evidence in the low-temperature diffraction data to suggest a lowering of the cell symmetry from tetragonal to orthorhombic. A noncollinear model consistent with the tetragonal symmetry was therefore considered. Based on arguments previously discussed in detail for this order [10,18], a noncollinear La_2CuO_4-type model ($P4_2/nn'm$ symmetry) has been adopted and the magnetic order is shown in Fig. 6. In contrast to the magnetic structure reported for $LaSrCoO_{3.5-x}$ [10], no evidence was found for a magnetic component parallel to the z-axis. The fits to the low-temperature NPD data are shown in Fig. 5 with refined structural parameters given in Table 3; an average of Fe^{3+} and Co^{2+} form factors was used in the refinements. The magnetic moments refined from the proposed model are 3.37(6) and 3.46(3) μ_B for LA1-red and LA12-red, respectively.

No evidence of AFM ordering has been observed in the low-temperature NPD data of the oxidized materials. Plots of the reciprocal of the molar susceptibility against temperature for these samples (LA1-ox and LA12-ox) (Fig. 7) suggest a nonCurie–Weiss behaviour in the given temperature range. The plots

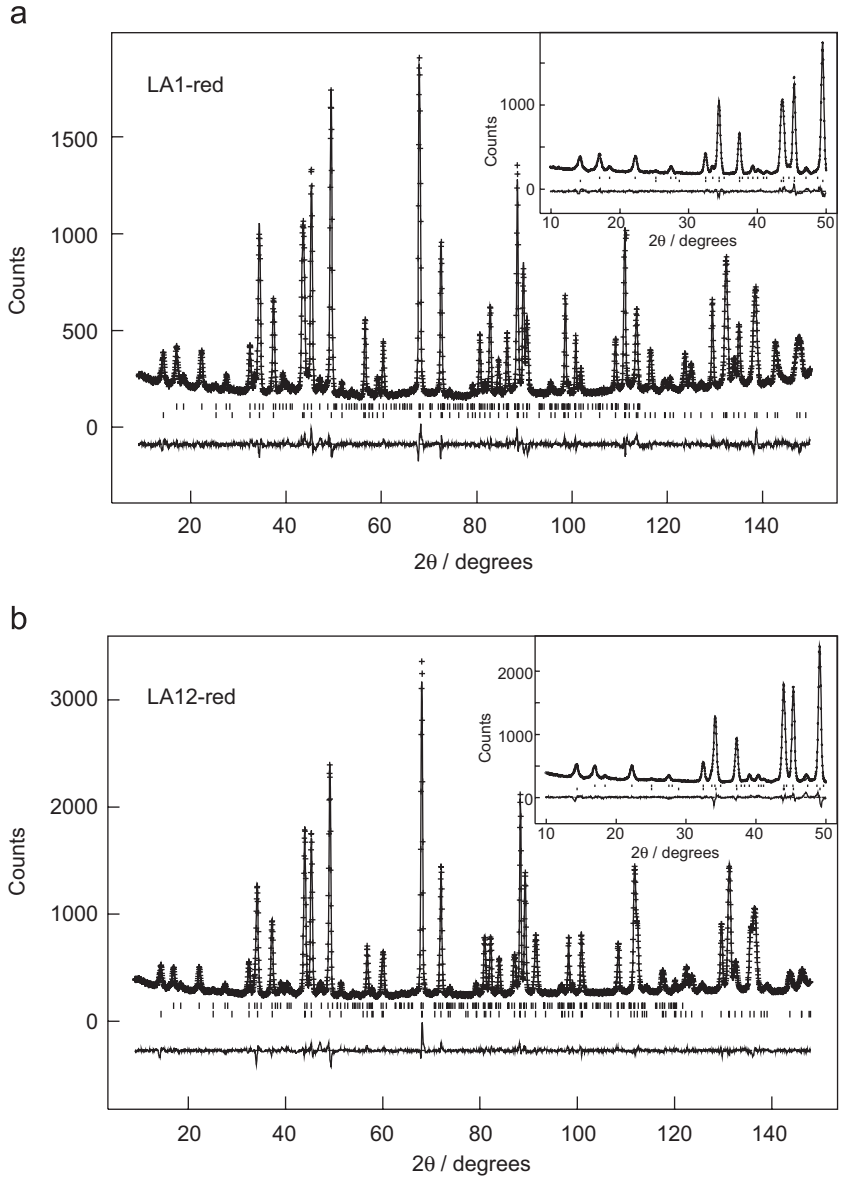

Fig. 5. Observed, calculated and difference profiles for NPD data collected at 5 K for (a) LA1-red and (b) LA12-red showing nuclear (lower tick marks) and magnetic (upper tick marks) reflections.

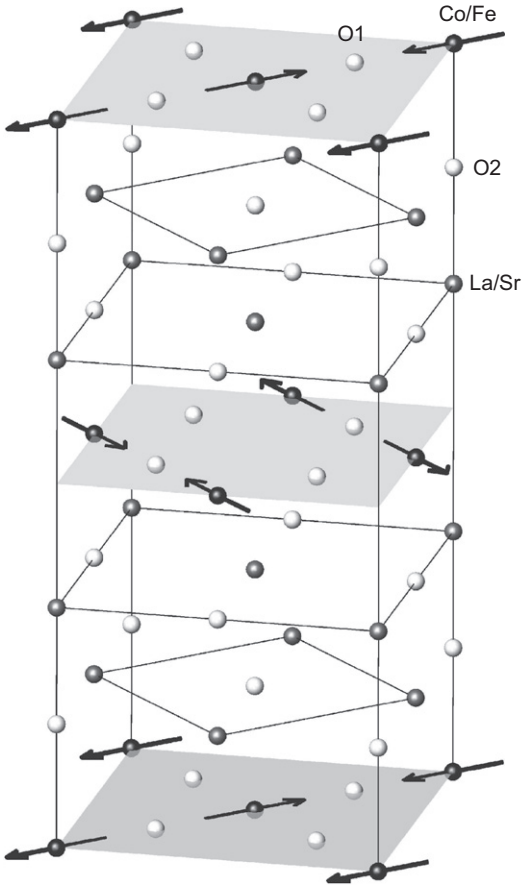

Fig. 6. Magnetic structure of the reduced samples. The arrows indicate the direction of Co/Fe magnetic moments.

display an increased gradient at low temperature, which is consistent with magnetic frustration [21]. Application of Curie–Weiss law at the extreme parts of the plots resulted in negative θ values and a decreasing effective moment as the temperature decreases; this is consistent with exchange interactions, which are predominantly AFM. Above 250 K, the θ values are −244.7 and −239.2 and the effective moments are 3.37 and 3.47 μ_B, for LA1-ox and LA12-ox, respectively; the effective moments are too small to be due to high-spin Fe^{3+} and Co^{3+}/Co^{2+} ions, which would provide effective magnetic moments of 5.43 and 5.26 μ_B for LA1-ox and LA12-ox.

4. Discussion

We have studied structural and magnetic properties of $LaSrCo_{0.5}Fe_{0.5}O_4$ and $La_{1.2}Sr_{0.8}Co_{0.5}Fe_{0.5}O_4$ (oxidized materials) and their reduced forms $LaSrCo_{0.5}Fe_{0.5}O_{3.75}$ and $La_{1.2}Sr_{0.8}Co_{0.5}Fe_{0.5}O_{3.85}$. The reduced phases show long-range AFM ordering at low temperature and the Néel transition temperatures seem to be close to room temperature. On the other hand, the oxidized materials (containing excess Co^{3+} ions) showed no evidence of ordering at low temperature, and the nonCurie–Weiss behaviour is suggestive of an AFM spin glass. The strong AFM coupling in the reduced samples can be readily explained by the presence of Co^{2+} ($t_{2g}^5\ e_g^2$) and Fe^{3+} ($t_{2g}^3\ e_g^2$), for which AFM exchange is expected for all 180° superexchange interactions. For the oxidized phases, the magnetic behaviour can be attributed to competing AFM and FM interactions, which supports the presence of Co^{3+} ions in the low-spin state, Co^{3+} ($t_{2g}^6\ e_g^0$). A disordered Co/Fe

Table 3
Structural results for the refinement of the neutron diffraction data collected at 5 K

Atom	x	y	z	$100 \times U_{iso}$ (Å^2)	Occupancy	x	y	z	$100 \times U_{iso}$ (Å^2)	Occupancy
LA1-red: space groups *I*4/*mmm* (nuclear) and $P4_2/nn'm$ (magnetic)						LA12-red: space groups *I*4/*mmm* (nuclear) and $P4_2/nn'm$ (magnetic)				
Co/Fe	0	0	0	0.373(3)	0.5/0.5	0	0	0	0**	0.5/0.5
La/Sr	0	0	0.3574(6)	0.464(2)	0.5/0.5	0	0	0.3589(6)	0.015(2)	0.6/0.4
O1	0.5	0.0471(7)	0	0.66(5)	0.441(2)	0.5	0.0344(8)	0	0.01(5)	0.465(2)
O2	0	0	0.1690(7)	1.32*	1	0	0	0.1711(4)	1.12*	1
*U_{11} = 1.61(4) Å^2; U_{22} = 1.61(4) Å^2; U_{33} = 0.74(8) Å^2						*U_{11} = 1.18(4) Å^2; U_{22} = 1.18(4) Å^2; U_{33} = 1.01(1) Å^2				
						**Negative U_{iso} constrained to zero.				
a = 3.81536(8) Å; c = 12.92629(3) Å						a = 3.84140(7) Å; c = 12.80634(3) Å				
Atom	x	y	z	M_x (μ_B)	M_y(μ_B)	M_z (μ_B)	|*M*| (μ_B)	x	y	z	M_x (μ_B)	M_y (μ_B)	M_z (μ_B)	|*M*| (μ_B)
Co/Fe	0	0	0	2.38(7)	2.38(7)	0	3.37(6)	0	0	0	2.44(9)	2.44(9)	0	3.46(3)
wRp = 0.0395; Rp = 0.0305; χ^2 = 3.741								wRp = 0.0340; Rp = 0.0248; χ^2 = 4.019						

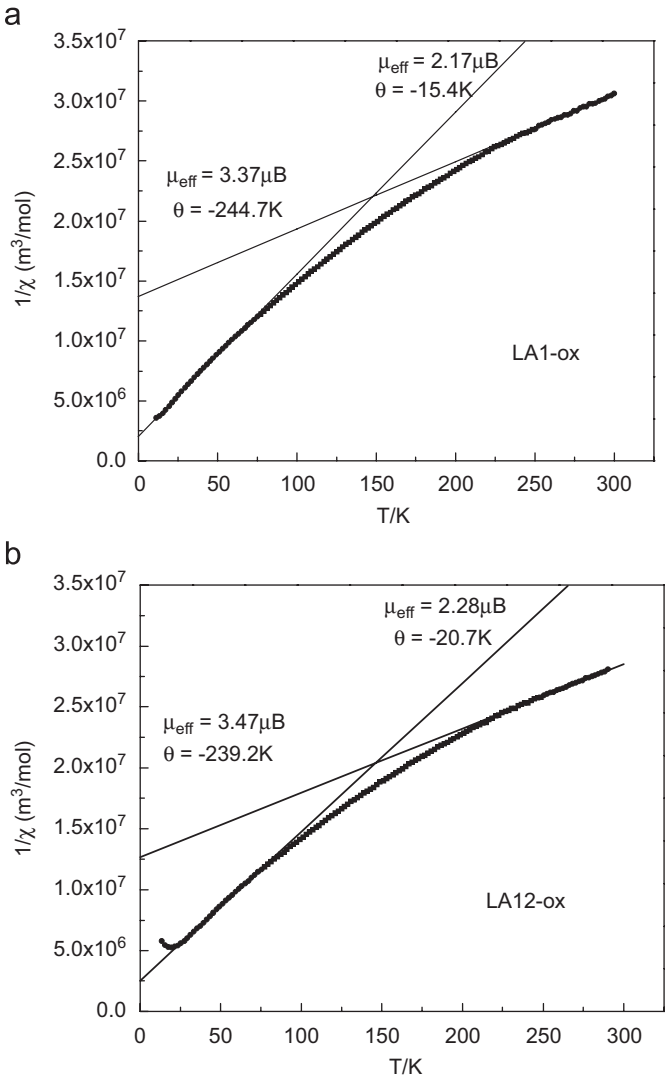

Fig. 7. Variation of the inverse magnetic susceptibilities (ZFC) with temperature for LA1-ox and LA12-ox.

distribution would result in competing FM (Co–Fe) and AFM (Co–Co and Fe–Fe) interactions. Low-spin Co^{3+} is generally agreed to be the ground state in $LaCoO_3$ [22], and recent studies have suggested that the ground state of $LaSrCoO_4$ is the low spin–high spin (LS–HS)-ordered state rather than the intermediate state (IS) [23].

The ordering scheme shown in Fig. 6 is used to account for the AFM coupling between Fe^{3+}/Co^{2+} spins in the reduced samples. The ordered moments refined from the proposed model (3.37(6) and 3.46(3) μ_B for LA1-red and LA12-red, respectively) are ~15% lower than the expected moments for a mixture of high-spin Fe^{3+} and Co^{2+} assuming only a spin contribution to the moment ($g = 2.0$). This reduction is less than might be expected from the cumulative effects of covalence, the low dimensionality of the magnetic order and quantum mechanical effects. However, Co^{2+} ions have a significant orbital contribution that enhances the moment, and an experimental moment very close to the theoretical value of 3.0 μ_B has been reported for La_2CoO_4 [24]. The higher moment for Fe^{3+} (theoretical 5.0 μ_B) rationalizes the higher moments observed for LA1-red and LA12-red. The effective magnetic moments observed in the oxidized materials near room temperature (3.37 and 3.47 μ_B, for LA1-ox and LA12-ox, respectively) are somewhat lower than those expected from high-spin Fe^{3+}/Co^{2+} and low-spin Co^{3+} (4.18 and 4.53 μ_B), but the data are not in a Curie–Weiss regime.

A lattice expansion can be observed through the electron-doping of stoichiometric $LaSrCo_{0.5}Fe_{0.5}O_4$ to form $La_{1.2}Sr_{0.8}Co_{0.5}Fe_{0.5}O_4$ (lattice parameters are $a = 3.83900(6)$; $c = 12.56764(2)$ and $a = 3.85523(6)$; $c = 12.60714(2)$, respectively). This expansion results from an increase in the B-site ionic radius owing to replacement of some LS Co^{3+} by HS Co^{2+}, and this effect is larger than the contraction expected for partial replacement of Sr^{2+} by La^{3+}.

Oxide ion vacancies in the reduced phases ($LaSrCo_{0.5}Fe_{0.5}O_{3.75}$ and $La_{1.2}Sr_{0.8}Co_{0.5}Fe_{0.5}O_{3.85}$) are located within the MO_2 (M = Co/Fe) planes of the K_2NiF_4 structure. These phases are obtained via reduction of Co^{3+} ions to Co^{2+} ions, associated with a significant expansion in the c parameter (3.15% and 1.85%) and a slight contraction in the a parameter (0.4% and 0.16%, respectively). A similar effect has been observed under reduction of $LaSrCoO_4$ into $LaSrCoO_{3.5-x}$ [10]. The expansion and contraction are both proportional to the amount of Co^{3+} being reduced to Co^{2+} (i.e. the amount of oxygen vacancies). The expansion in c corresponds to a significant expansion in the M–O2 bond length (e.g. M–O2 is 2.085(5) and 2.220(1) Å in LA1-ox and LA1-red, respectively), while no significant contraction has been observed in the M–O1 bond (e.g. M–O1 is 1.919(5) and 1.921(8) Å in LA1-ox and LA1-red, respectively). This effect can be attributed to the rotation of the MO_6 octahedra around the z-axis to maintain the M–O1 bond lengths, whilst allowing contraction of a. This effect is reflected in the increase in the O1 y parameter for LA1-red, 0.0509(6), compared with LA12-red, 0.0333(7) (Table 1).

An expansion in the MO_6 octahedra is generally expected under reduction of Co^{3+} to Co^{2+}, which explains the expansion in the c parameter. The contraction in a, however, is often related to the coordination requirements of the A site (La/Sr); under reduction, a contraction in the coordination sphere (achieved in the xy plane, i.e. La/Sr–O_{axial} bonds) occurs due to reduction of coordination number (<9). This effect is seen in $LaSrCoO_{3.5-x}$ via small contraction in La/Sr–O_{axial} bond lengths under reduction [10], which is not significant in this study, possibly because of (i) the a parameter contraction in our system is significantly lower than that observed in $LaSrCoO_{3.5-x}$ since the oxygen deficiency is lower, (ii) a slight contraction in La/Sr–O_{axial} bond lengths here may be screened by the anisotropic displacement adopted to the O2 (axial) oxygen sites.

Finally, rotation of the MO_6 octahedra around z in the reduced samples may produce an anisotropic strain within the lattice and account for the necessity to use Finger–Cox–Jephcoat functions in refining the peak shapes for these phases.

5. Conclusions

The phases $LaSrCo_{0.5}Fe_{0.5}O_{4-\delta}$ and $La_{1.2}Sr_{0.8}Co_{0.5}Fe_{0.5}O_{4-\delta}$ crystallize in a tetragonal K_2NiF_4 structure (space group $I4/mmm$). Oxide ion vacancies in oxygen-deficient phases are randomly distributed within the equatorial planes of the K_2NiF_4 structure with an associated contraction in the a parameter (compared with the stoichiometric materials) and a rotation of the (Co/Fe)O_6 octahedra around the z-axis. Iron is in the trivalent state in these materials. Co^{2+}-containing phases ($LaSrCo_{0.5}Fe_{0.5}O_{3.75}$ and $La_{1.2}Sr_{0.8}Co_{0.5}Fe_{0.5}O_{3.85}$) are antiferromagnetically ordered at low temperature. The AFM coupling results in a noncollinear scheme of ordering consistent with the tetragonal symmetry. Co^{3+} ions in $LaSrCo_{0.5}Fe_{0.5}O_4$ and $La_{1.2}Sr_{0.8}Co_{0.5}Fe_{0.5}O_4$ are assumed to be in the low-spin state and provide competing

FM and AFM exchange and the absence of long-range magnetic order in these phases.

Acknowledgments

We thank the Egyptian Education Bureau (London) for financial support (H. El Shinawi). We are also grateful to F.J. Berry for the provision and interpretation of Mössbauer spectra and E. Suard for assistance with the collection of NPD data.

References

[1] Y. Teraoka, H.M. Zhang, K. Okamoto, N. Yamazoe, Mater. Res. Bull. 23 (1988) 51–58.
[2] Y. Teraoka, H.M. Zhang, S. Furukawa, N. Yamazoe, Chem. Lett. 14 (1985) 1743–1746.
[3] Y. Matsumoto, S. Yamada, T. Nishida, E. Sato, J. Electrochem. Soc. 127 (1980) 2360–2364.
[4] S.E. Dann, M.T. Weller, D.B. Currie, J. Solid State Chem. 97 (1992) 179–185.
[5] F. Prado, T. Armstrong, A. Caneiro, A. Manthiram, J. Electrochem. Soc. 148 (2001) J7–J14.
[6] Y. Bréard, C. Michel, M. Hervieu, F. Studer, A. Maignan, B.B. Raveau, Chem. Mater. 14 (2002) 3128–3135.
[7] A. Bowman, M. Allix, D. Pelloquin, M.J. Rosseinsky, J. Am. Chem. Soc. 128 (2006) 12606–12607.
[8] A. Tabuchi, H. Kawanaka, H. Bando, T. Sasaki, Y. Nishihara, J. Alloy. Compd. 424 (2006) 21–26.
[9] A.C. Larson, R.B. Von Dreele, General Structural Analysis System, Los Alamos National Laboratory, Los Alamos, NM, 1994.
[10] M.A. Hayward, M.J. Rosseinsky, Chem. Mater. 12 (2000) 2182–2195.
[11] M.E. Leonowicz, K.R. Poeppelmeier, J.M. Longo, J. Solid State Chem. 59 (1985) 71–80.
[12] M. Crespin, J.M. Bassat, P. Odier, P. Mouron, J. Choisnet, J. Solid State Chem. 84 (1990) 165–170.
[13] P.H. Labbe, M. Ledesert, V. Caignaert, B. Raveau, J. Solid State Chem. 91 (1991) 362–369.
[14] F. Menil, J. Phys. Chem. Solids 46 (1985) 763–789.
[15] J.L. Soubeyroux, P. Courbin, L. Fournes, D. Fruchart, G. Le Flem, J. Solid State Chem. 31 (1980) 313–320.
[16] A. Nemudry, P. Rudolf, R. Schollhorn, Solid State Ionics 109 (1998) 213–222.
[17] D.E. Cox, A.I. Goldman, M.A. Subramanian, J. Gopalakrishnan, A.W. Sleight, Phys. Rev. B 40 (1989) 6998–7004.
[18] A.L. Hector, C.S. Knee, A.I. MacDonald, D.J. Price, M.T. Weller, J. Mater. Chem. 15 (2005) 3093–3103.
[19] M.M. Nguyen-Trut-Dinh, M. Vlasse, M. Perrin, G. Le Flem, J. Solid State Chem. 32 (1980) 1–8.
[20] M.H. Jung, A.M. Alsmadi, S. Chang, M.R. Fitzsimmons, Y. Zhao, A.H. Lacerda, H. Kawanaka, S. El-Khatib, H. Nakotte, J. Appl. Phys. 97 (2005) 10A926.
[21] K.V. Rao, M. Fahnle, E. Figueroa, O. Beckman, L. Hedman, Phys. Rev. B 27 (1983) 3104–3107.
[22] M.A. Senaris-Rodriguez, J.B. Goodenough, J. Solid State Chem. 116 (1995) 224–231.
[23] J. Wang, W. Zhang, D.Y. Xing, Phys. Rev. B 62 (2000) 14140–14144.
[24] K. Yamada, M. Matsuda, Y. Endoh, B. Keimer, R.J. Birgenau, S. Onedera, J. Mizusaki, T. Matsuura, G. Shirane, Phys. Rev. B 39 (1989) 2336–2343.